CHAPTER IV

MAGNETICALLY CONTROLLED MICROFLUIDIC TUNING FOR FREQUENCY RECONFIGURATION IN PLANAR GEOMETRY

4.1 Introduction

Microfluidic channel based tuning shows growing interests in reconfiguring the antenna operating characteristics [1-4]. Most of these approaches use liquid metal as antenna radiators or parasitically coupled elements to achieve effective, less interfering and reliable reconfiguration [5]. The desired tunings are achieved through controlled actuation of the liquids used [6-12].

This chapter presents a technique to tune antenna resonating frequency by changing the dielectric behaviour of the substrate material underneath the radiating patch. The technique uses microfluidic channels embedded into the antenna substrate. The channels are filled with two immiscible liquids of different permittivity values. A spatial variation in the dielectric constant value is obtained by changing the relative positions of the fluids. The required actuation is provided electromagnetically through a contactless mechanism. For the proposed electromagnetic actuation, one of the liquids selected is magnetic in nature.

The first section of the chapter presents the design and development of microfluidic switch including the choice of fluids and their characterizations. The following sections focus on the development of an antenna substrate with embedded microfluidic channels and finally, the performance of the prototype antenna is verified.

4.2 Development of magnetically controlled microfluidic switch

The microfluidic switching system uses two liquids of sufficiently varying permittivity to construct a tuning mechanism for frequency reconfiguration. Hence, the choice of liquids with suitable properties are crucial.

As the work uses two liquids to construct a tuning mechanism for frequency reconfiguration; it is crucial to use liquids with suitable properties. A magnetic dispersion (ferrofluid) is chosen as one of the fluids, for its dependency towards an external magnetic field. Due to this property, the position of ferrofluid (FF) can be changed externally without connecting any mechanical pumps. From the

design perspective, this is a significant advantage, as mechanical pumps require additional controllers and tubing which make the overall system clumsy [5, 13].

A solution of Isopropanol in deionized water (ISPW) is chosen as the second liquid to provide a necessary variation of dielectric constant. ISPW solution also provides a slip layer in between the microfluidic channel wall and FF, which reduces the surface wettability of FF. Thus, ensures a smooth flow through the channel.

The ferrofluid used in this work is a colloidal dispersion of magnetite (Fe_3O_4) nanoparticles suspended in a hydrocarbon-based carrier fluid. Magnetite nanoparticles are first synthesized and characterized. The nanoparticles are added to a carrier fluid to form the ferrofluid. FF and ISPW solutions are thereafter characterized for their microwave properties and actuation speed.

4.2.1 Synthesis of magnetic nanoparticles

Magnetic (Fe_3O_4) nanoparticles are synthesized by co-precipitation technique [14, 15]. Precursor solutions of $FeCl_3$ and $FeCl_2$ are taken in the molar ratio of 0.5 and then added concurrently to a 0.4 N HCl solution of volume 25 ml. A 1.5 N solution of NaOH is prepared and added to the resulting solution under constant stirring while maintaining the pH of the final solution at 12. The process results in a dark black precipitate. Impurity free precipitate of magnetic nanoparticles is obtained after repeated washing and centrifugation. In order to stop further oxidation a 0.01 N HCL is added to the sample. Synthesized magnetic nanoparticles are then coated with a surfactant layer. Approximately 400 µl of anionic surfactant oleic acid [$C_{18}H_{34}O_2$, 99% pure, Otto] is added to the sample under vigorous stirring.

4.2.2 Characterization of magnetic nanoparticles

X-Ray diffraction

The microstructure of oleic acid coated nanoparticles is studied by an X-ray diffractometer (Rigaku Mini Flex 2000). Figure 4.1 (a) shows X-ray diffractogram of the nanoparticles and the pattern exhibit (220), (311), (511) and (440) diffraction

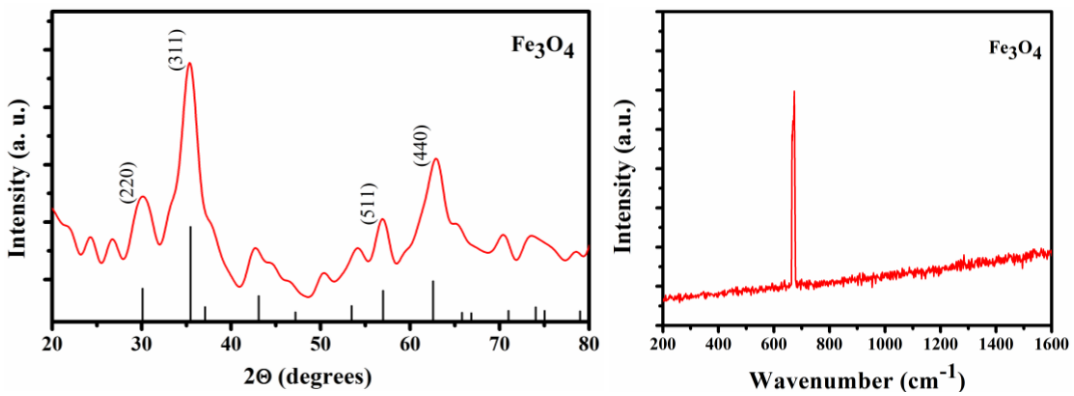

(a) (b)

Figure 4.1 (a) XRD difractogram of Fe_3O_4 (FFT smoothed) (b) Raman spectra of Fe_3O_4 nanoparticles

peak of Fe_3O_4. Considering the positions and relative intensities the planes can be indexed to Fe_3O_4 with cubic structure (JCPDS card no 65-3107).

A pattern decomposition procedure using a pseudo-Voigt profile shaped function and subsequent single-line analysis based on the equivalent Voigt representation is used for the determination of average crystallite size and lattice strain.

$$D = \frac{\lambda}{\beta_c^f \cos\theta}$$

$$e = \frac{\beta_g^f}{4\tan\theta}$$

where λ is the wavelength of the X-ray, β_c^f and β_g^f are the integral breadths of the Cauchy and Gaussian fit of the structurally broadened profile and θ is the Bragg angle. The average crystallite size, estimated using single line analysis considering the most prominent peak (311) is found to be 7.6 nm and corresponding lattice strain is 0.0087.

Raman spectroscopy

The Raman spectra of the sample is recorded using a Laser Micro Raman System (LabRam HR) with Ar+ laser excitation source of wavelength 514.5 nm. The Raman spectrum is revealed in Figure 4.1 (b). The nanoparticles show a peak around 667 cm^{-1}, which is in agreement with the reported typical value of magnetite (Fe_3O_4) in the literature (661cm^{-1}) [16].

Transmission electron microscopy (TEM)

Transmission electron microscopy (TEM) is taken using an FEI COMPANY TECNAI G2 20 S-TWIN (200KV) electron microscope operating at an accelerating voltage of 200 kV. For TEM, the powder samples are dispersed in n-hexane followed by ultrasonication for 10 min. After that, a few drops of the dispersion is taken on a carbon-coated copper grid and dried at room temperature. The size distributions of the nanoparticles are estimated based on the statistics of 200 particles chosen from multiple images. Magnified images (Figure 4.2 (a)) show the primary particles of average size of 6 nm.

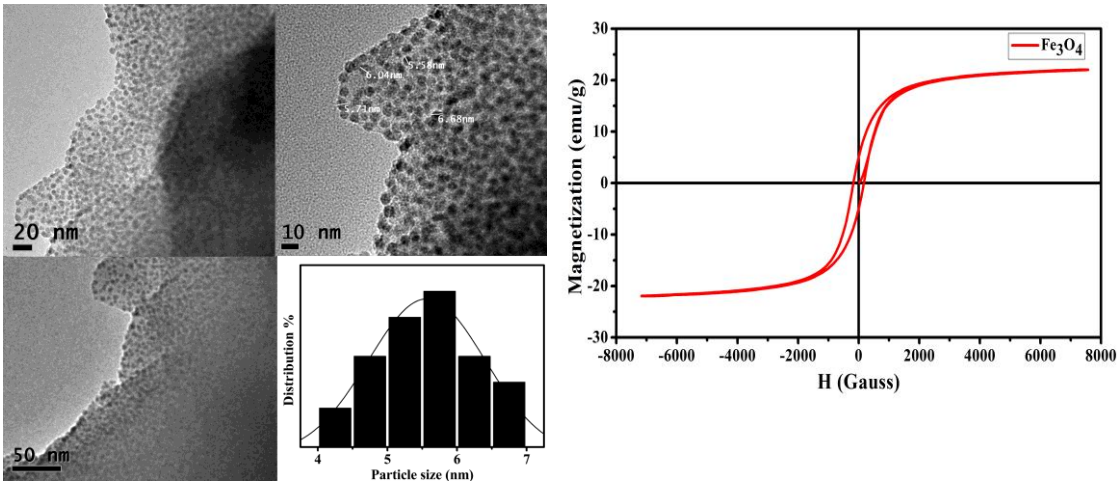

(a) (b)

Figure 4.2 (a) TEM images of Fe_3O_4 nanoparticles, (b) Hysteresis loop of Fe_3O_4 nanoparticles

Vibrating sample magnetometry

The magnetic behavior of the Fe_3O_4 nanoparticles is characterized by using vibrating sample magnetometer (VSM, LakeShore Model 7410) by performing magnetic hysteresis loops (M-H) at room temperature 300 K. Figure 4.2 (b) shows the M-H curve of the nanoparticles with a coercivity of 173.18 G and saturation magnetization 21.986 emu/g.

Microwave characterization

Transmission reflection line (TRL) technique [17, 18] is used for determining complex permittivity the Fe_3O_4 nanoparticle over a frequency range of 4.0 GHz –

10.00 GHz. A 3.5 mm coaxial air-line with a length of 70 mm is used as the transmission line. A cylindrical sample of outer diameter 3.5 mm, inner diameter 1.5 mm and length 5 mm is inserted inside the coaxial airline sample holder [19]. The transmission (S21) and reflection (S11) parameter are measured using Agilent E8362C Vector Network Analyzer (VNA). The complex permittivity ($\varepsilon_r = \varepsilon_r' - \varepsilon_r''$) is computed using Agilent 85071E material measurement software based on Nicolson-Ross technique [20, 21]. The measured real part of permittivity, ε_r' and dielectric loss ($tan\ \delta = \varepsilon_r''/\varepsilon_r'$) is shown in Figure 4.3 (a) and (b), respectively.

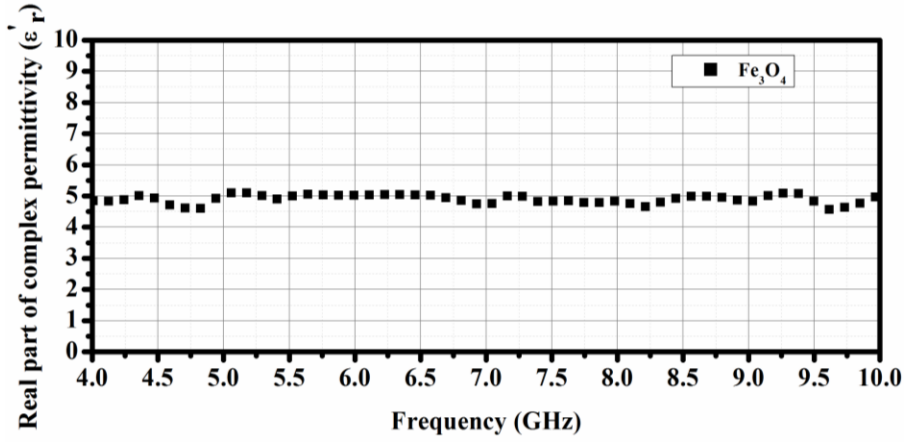

(a)

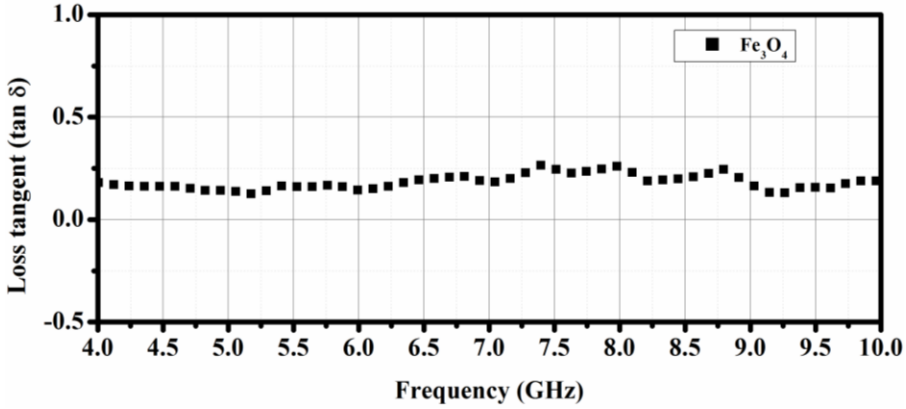

(b)

Figure 4.3 (a) Real part of complex permittivity, ε_r' and (b) loss tangent $tan\ \delta$

The ε_r' and tan δ does not show much variation with frequency over the range. ε_r' varies between 4.6 – 5.0 , while $tan\ \delta$ is ~ 0.28.

4.2.3 Synthesis and characterization of the fluids

Ferrofluid is synthesized by dispersing the surfactant coated of magnetite (Fe_3O_4) nanoparticles to a hydrocarbon-based carrier fluid, hexane in a concentration of ~ 6.6 % wt/vol. The dispersion is ultra-sonicated for 2 hours for the homogeneous spreading of the nanoparticles. ISPW solution is prepared by mixing analytical grade isopropanol and deionized water in a 3:1 ratio.

The prepared ferrofluid and the ISPW solution are then studied for their microwave as well as some physical properties and details are given below.

Microwave characterization of fluids

Microwave characterizations of the prepared FF and ISPW solution are carried out using Keysight dielectric probe system, which is connected to the Agilent VNA. Figure 4.4 presents the measured real parts of the permittivity along with the loss tangent values for the range 4.0 GHz – 10.0 GHz.

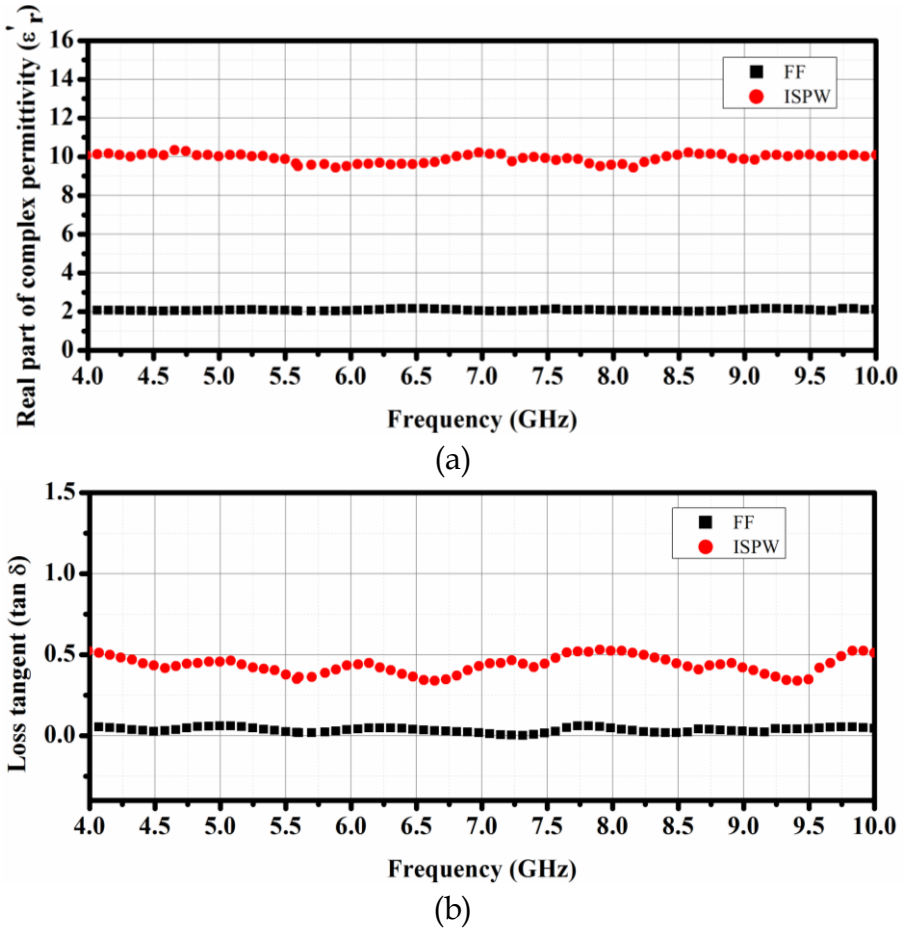

Figure 4.4 (a) Real part of permittivity and (b) loss tangent of FF and ISPW solution

Dielectric constant is around 2.02 for FF and 9.86 for ISPW solution. The loss tangent of FF is around 0.02 while the ISPW solution shows a relatively higher loss with loss tangent ~ 0.48.

Actuation Speed Test

The actuation speed test is performed to study the speed of FF immersed in ISPW mixture, under an external magnetic field. Both the liquids are encapsulated in a capillary of diameter ~ 0.8 mm. The test is performed using a linear channel, a video camera with a capture rate of 120 fps and an electromagnet. A video is recorded at a rate of 120 fps when FF is under a translational motion from position A (0 – 11 mm) to B (11 – 22 mm). The video file is then processed and frames are extracted. Sequential frames are analyzed in the ImageJ software. The result reveals an actuation speed is up to 110.82 mm/s and the total transmission time of 358.19 milliseconds for a shifting distance of ~ 12.00 mm (Figure 4.5). The images also confirm the reduced wettability of FF as there is no residue left behind after the transmission.

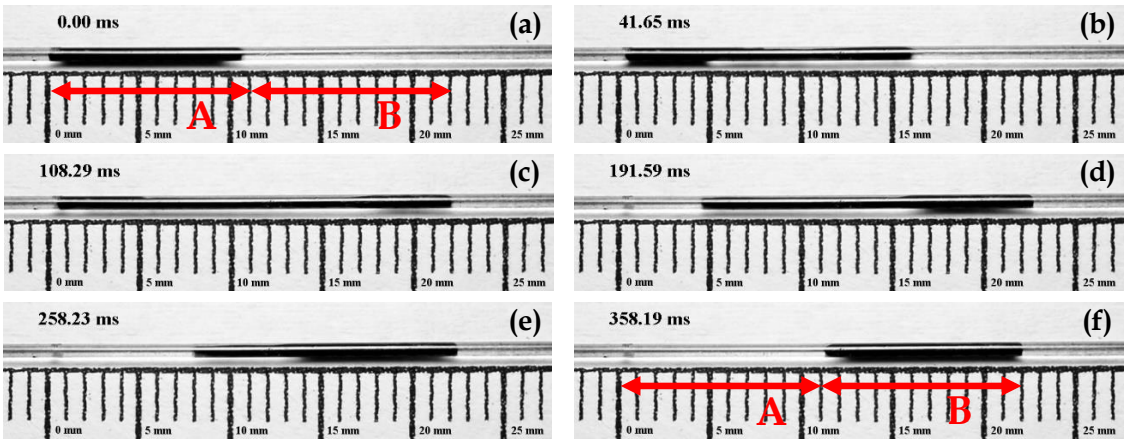

Figure 4.5 Sequential image analysis of the fluid transmission process. During the actuation a portion of FF (black fluid) covers a distance of ~ 12.00 mm in 108.29 milliseconds and completely shifts to the new position in 358.19 milliseconds.

Contact angle measurement

As the ferrofluid (FF) has a high degree of surface wettability, measures are taken to reduce the wettability. The surface of the microchannels, where fluids are to be injected is coated with an oleophobic solution to minimize the wettability. To mark

the amount of reduction in the degree of wetting, contact angle measurements are carried out for oleo-phobic solution coated and non-coated surfaces, using a DataPhysics - OCA 15EC measuring device. At first, the measurement is taken on a non-coated fluorinated ethylene propylene (FEP) surface and then for an oleo-phobic solution coated FEP surface. From the recorded contact angel images, it is observed that with the coating the contact angles become obtuse angle; whereas for non-coated surface it is less than 90˚. The increased contact angle for the coated surface is an indication of the reduction in the degree of wetting. Figure 4.6 shows the contact angle images of the two surfaces and details are listed in Table 4.1. FEP surface is used for the testing as the microchannels used in the work is made up of FEP.

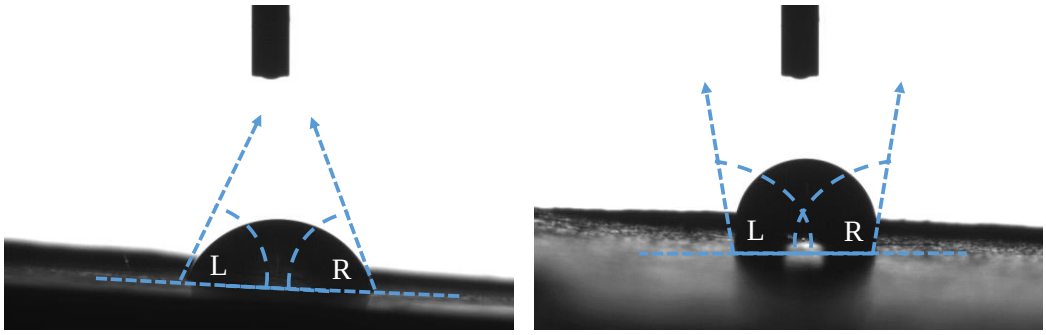

(a) (b)

Figure 4.6 Contact angle images of ferrofluid on (a) non-coated and (b) oleophobic solution coated FEP surface

Table 4.1 Contact angle measurement data

Sample	Left Angle L (˚)	Right Angle R (˚)
Non coated	66.8	66.9
Coated	101.6	101.8

4.3 Magnetically controlled frequency reconfigurable antenna

The work emphasizes on the reconfiguration of frequency in a planar geometry through a magnetically controlled mechanism. The design uses an engineered substrate to hold the mechanism.

4.3.1 Fabrication of microfluidic channel embedded substrate

The engineered substrate is a sandwich structure composed of microchannels embedded un-cladded FR4 slab of ε_r= 4.3 and thickness 1.4 mm and two copper

cladded comparatively thin FR4 layers. The middle sheet is engraved to house the fluorinated ethylene propylene (FEP) channels of the diameter approximating to 0.9 mm with a wall thickness of ~ 0.1 mm. The length of each channels is 24.88 mm. Two very thin (0.2 mm) single side copper cladded FR4 layers are glued to this modified section. A graphical representation of the process is shown in Figure 4.7.

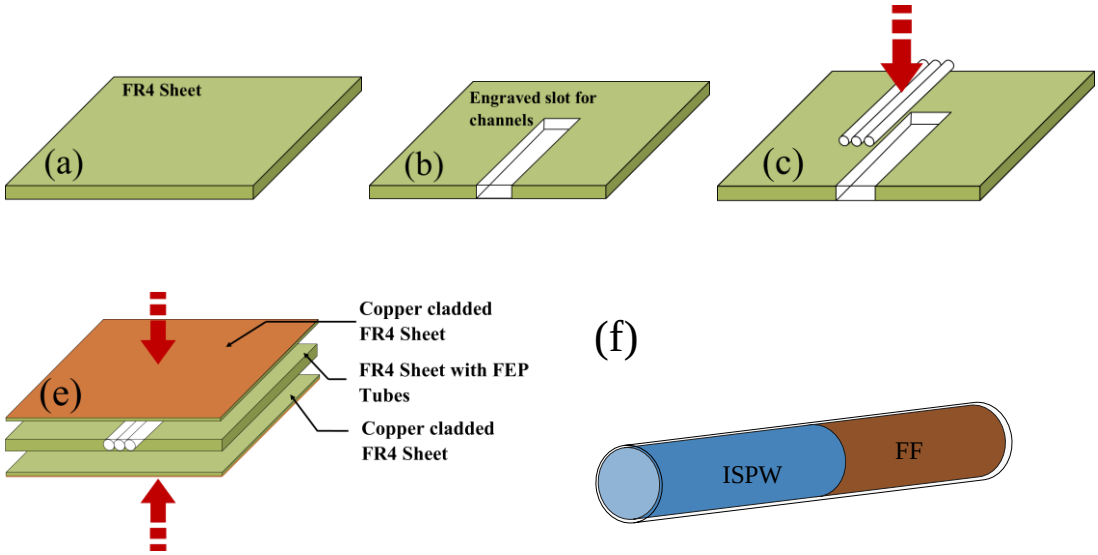

Figure 4.7 Schematic diagram of the substrate modification in sequences (a) to (e) and (f) fluidic channel with injected liquids

The channels are filled with the FF and ISPW solutions mentioned in the previous section. The tubes are first filled with the mixture of isopropanol and deionized water (ISPW) and then a part of the solution is replaced by the synthesized ferrofluid. While filling the tubes, it is confirmed that no air bubble is formed inside the channels. The volume occupied by each of the liquids are equal and covers a tube length of ~ 12.44 mm. Tubes are sealed properly once they are completely filled. Prior to filling the fluids, the FEP channels are coated with oleo-phobic solutions to reduce the surface wettability of ferrofluid.

4.3.2 Design and fabrication of the frequency reconfigurable antenna

The antenna pattern is etched on one of these copper cladded sides while the opposite side acts as the ground plane. It is a rectangular microstrip patch and is edge fed using a 50 Ω microstrip line with a quarter wave transformer. Antenna patch dimensions are calculated to resonate at 7.60 GHz, for FR4 substrate of

thickness 1.8 mm (the thickness is kept same as the sandwiched structure). The design scheme of the modified substrate and placing of the antenna is presented in Figure 4.8. It is well known that in RMA, fringing field line concentrations are maximum at the patch edges and hence, maximum penetration into the substrate occurs across the edges [22, 23]. The FEP tubes are placed just beneath the radiating edge, opposite to the feeding edge.

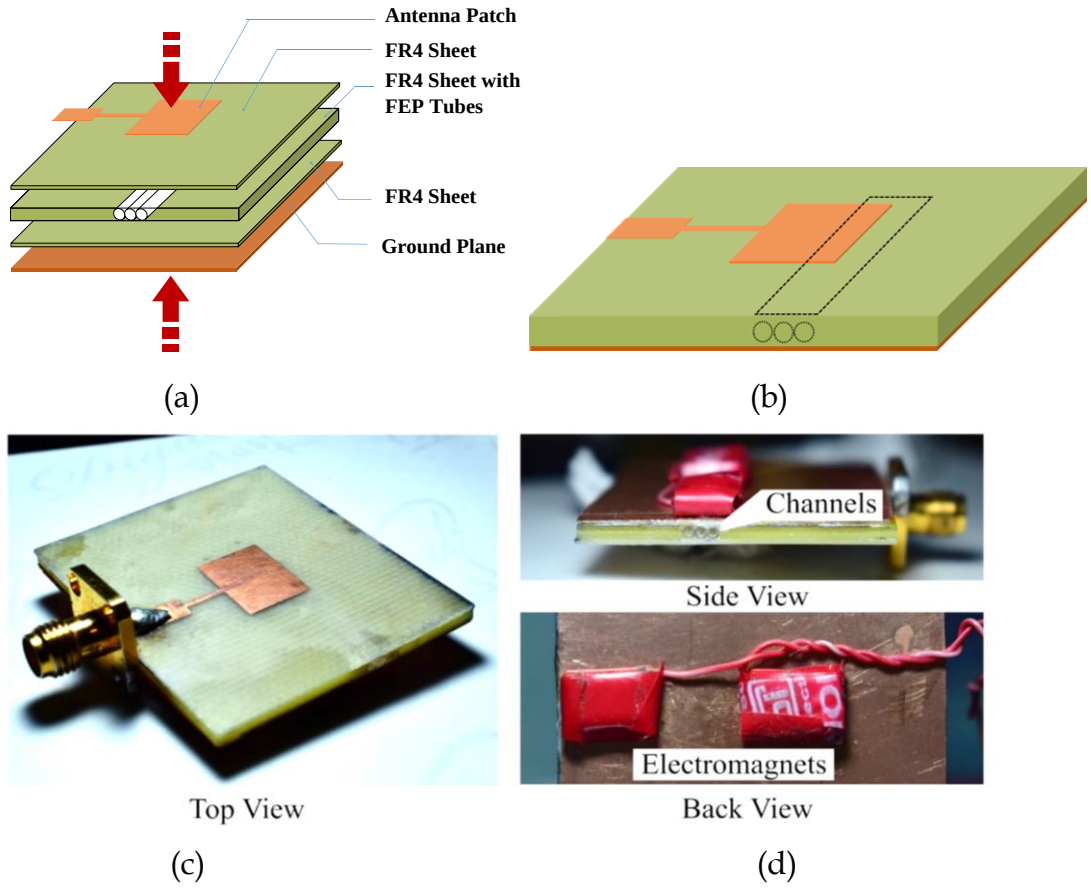

Figure 4.8 Fabrication scheme of the proposed antenna (a) Stacking of various layers (b) Final prototype with marked channel position (dotted lines) (c) Fabricated antenna (d) Three different viewing angle

To maximize the effect of spatially varying dielectric constant on the resonant frequency, three tubes are taken and positioned such that it covers the extended patch length, ΔL, occurred due to fringing [22]. The length of the channels is kept slightly larger than twice the patch width, W (here, it is about 24.88 mm). These extra millimetres are used to minimize the effect of the fluid positioned on the other end of the channel.

4.3.3 Mechanism of frequency reconfiguration with microfluidic channels

The targeted frequency reconfiguration is achieved through the lateral displacement of the liquids. The position of FF inside the channels can be easily controlled using electromagnets, which eventually relocates ISPW also. As both the immiscible liquids possess two different dielectric constant value, the dielectric constant of the substrate under the antenna patch gets modified by altering the liquid position. The process is illustrated in Figure 4.9.

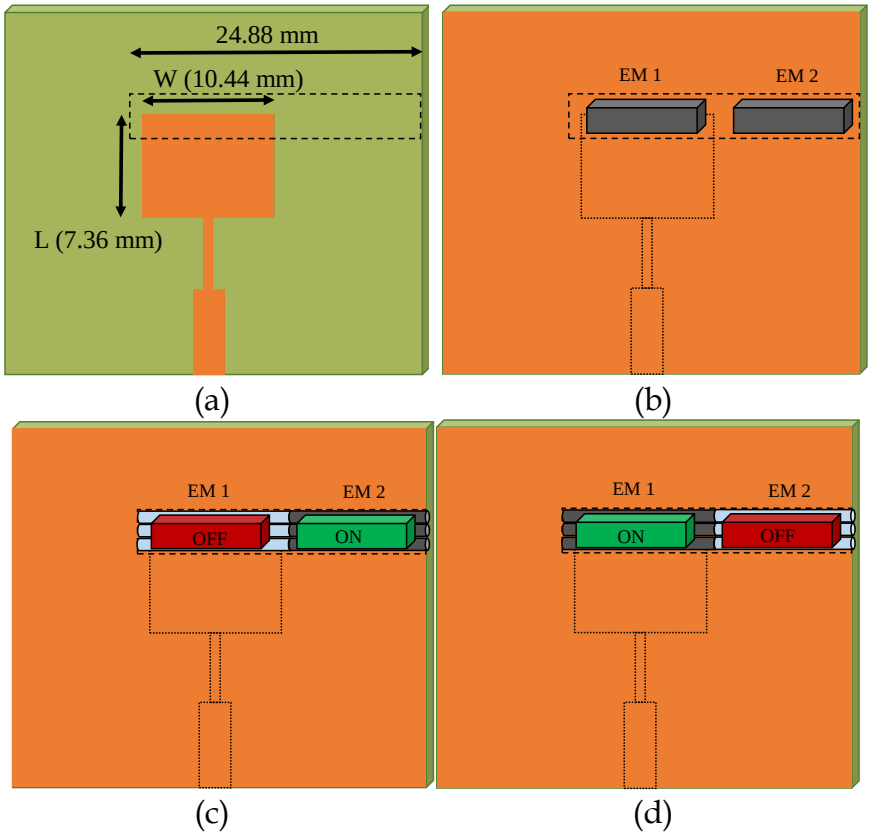

Figure 4.9 A depiction of the method that reconfigures the antenna resonant frequency: (a) Top view of the antenna with patch and channel dimension marked (b) Enlarged view showing the position of channels under the patch (c) Back view (ground plane) of the antenna showing the position of the electromagnets with patch position in dotted lines (d) Status of electromagnets and corresponding positioning of liquids (grey colour indicating FF and white colour ISPW).

Due to the interchanging of fluids underneath the radiating edge, the effective value of dielectric constant experienced by the patch changes and accordingly resonating frequency of the antenna shifts. Two electromagnets having a maximum strength of 400 Gauss are used to control the position of FF in the

channel. Thus the switching position can be altered from position A to position B and also reversed by activating the corresponding electromagnets.

4.4 Antenna performance study with microfluidic actuation

The fabricated antenna is tested for the targeted frequency reconfiguration. The frequency response of the antenna under various configurations are measured using an Agilent VNA (PNA E8362C). The reversible frequency shiftings are recorded by changing the ferrofluid's position. In Mode 1, FF is placed at position B (refer Figure 4.9 (d)) and ISPW at A by activating electromagnet EM 2. At this state, the antenna patch experiences a higher value of the dielectric constant and a resonating notch is observed at 7.40 GHz. A shift of 0.60 GHz is recorded in Mode 2 through the activation of EM 1. The recorded notch is at 8.00 GHz.

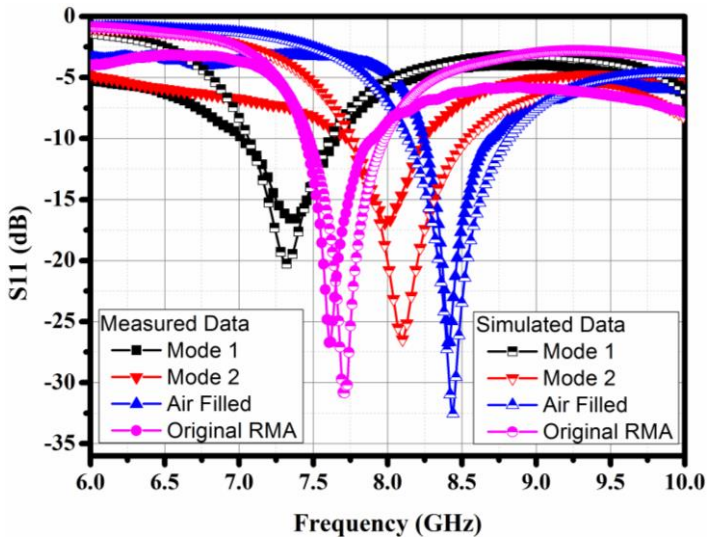

Figure 4.10 Two distinct frequency responses illustrating the frequency reconfigurability of the antenna between two modes. Responses of a standard RMA and antenna with air filled channels are also noticed. Solid symbol represents measured data and half-filled symbol represents simulated data.

To demonstrate the reversible frequency shifting, responses of the antenna at the sequential states are recorded by changing the ferrofluid's position. The resonant frequency of Mode 1 i.e. 7.40 GHz can be retrieved by again activating EM 2, which forces the ferrofluid to come into the position B. Similarly, Mode 2 also can be achieved by simply activating EM 1.

Simulation studies are also carried out. Both measured and simulated return losses (S11) are shown in Figure 4.10 with the detail presented in Table 4.2. The study also includes S11 parameters of an RMA on an unmodified substrate and with air-filled channel substrate. The original RMA resonates at 7.60 GHz and with the incorporation of the empty channels the frequency shifts to 8.40 GHz. The recorded -10 dB bandwidth for Mode 1 is 6.72 % and for Mode 2 it is 6.80 %.

Table 4.2 Resonating frequency, percentage bandwidth and gain at different substrate structure configuration

Mode	Electromagnet Status		Frequency (GHz)		% Bandwidth		Gain (dBi)
	EM 1	EM 2	Measured	Simulated	Measured	Simulated	
1	OFF	ON	7.40	7.38	6.72	7.61	3.20
2	ON	OFF	8.00	8.12	6.80	7.23	5.80
Antenna without channels	NA	NA	7.60	7.70	5.43	5.70	5.96
Air filled channels	NA	NA	8.40	8.48	5.50	6.75	6.21

From the return loss study, it is observed that for both the filled conditions, the frequency of the antenna shifts towards the lower side of the spectrum as compared to that of empty (air-filled) channel. Reason for this trend can be understood by considering the dielectric constant of the liquids in the microwave region and the basic equation of an RMA [22]. From Figure 4.4, FF dielectric constant is around 2.02, and 9.86 for ISPW mixture. With the fluids placed underneath the antenna radiator, the effective dielectric constant of the antenna substrate changes accordingly. For ISPW the value will be the highest and hence the lowest value of the frequency (7.40 GHz). Unmodified FR4 is positioned second with a dielectric constant 4.3, has a resonating notch at 7.60 GHz. In case of FF (ε_r =2.2), frequency is at 8.00 GHz. Air filled channels offer the lowest value of effective permittivity, as air has a dielectric constant nearly equal to 1 and results in a resonance at 8.40 GHz.

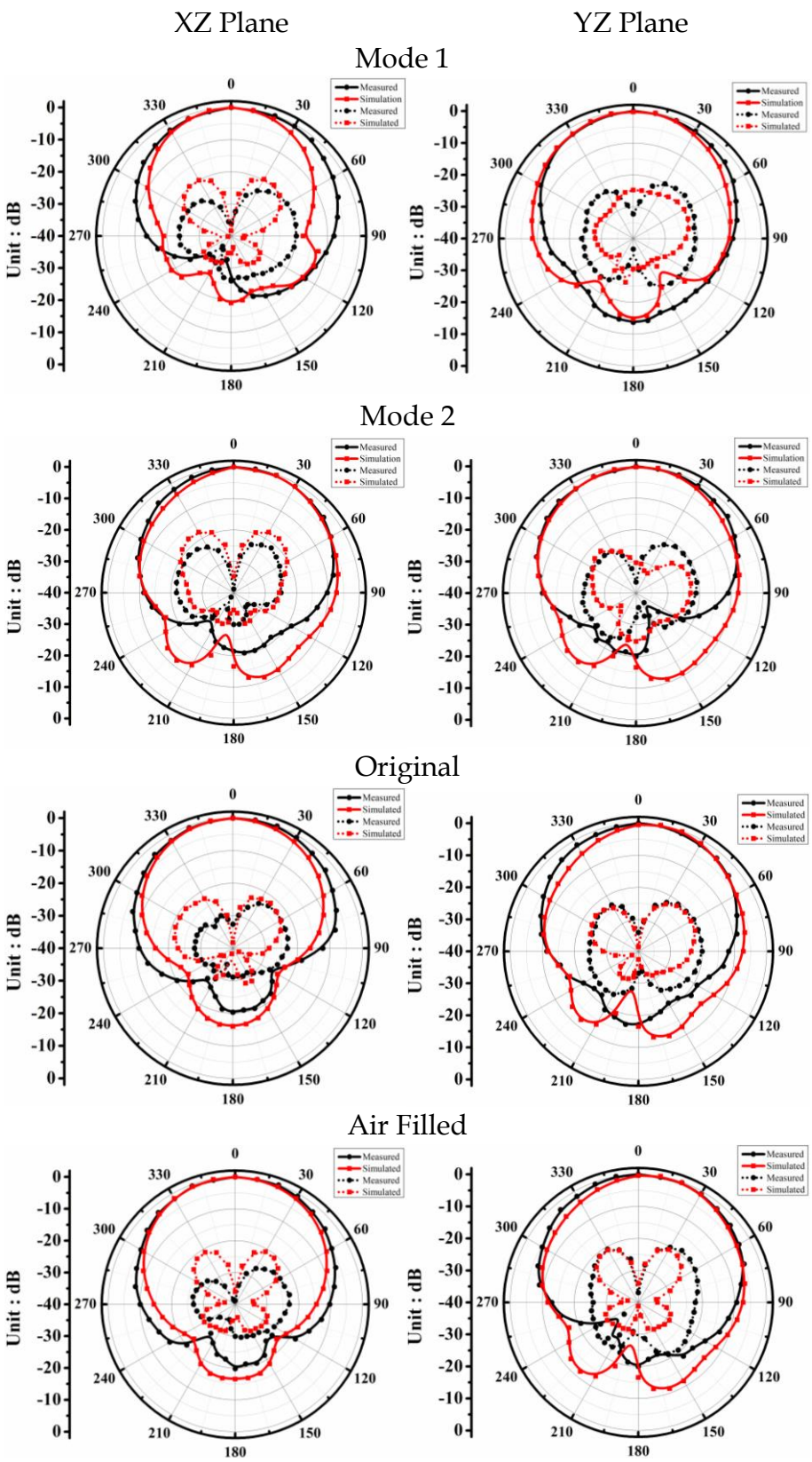

Figure 4.11 Radiation pattern in XZ plane (a) measured and (b) simulated and in YZ plane (c) measured and (d) simulated at resonant frequencies for different substrate structure

Radiation characteristics of the proposed antenna are also studied. Figure 4.11 shows measured and simulated radiation patterns of the antenna for both the reconfigured states, the air filled channel and original RMA. In the XZ plane, all the co-polarized patterns show the main lobe direction at 0° and 3 dB beamwidth of 96°. In YZ plane similar consistencies are observed with the main lobe direction at 5° and 3 dB beamwidth of 90°. The antenna offers low cross-polarization levels at all the frequencies. In Table 4.2 gain of the antenna for both the operating modes (Mode 1 and 2) along with the two other conditions are presented. The reduced gain of the antenna for the filled conditions compared to that of the air filled one is primarily due to the lossy nature of the fluids used. When the FF with a loss tangent of 0.04 is placed below the patch a gain of 5.80dBi is recorded at 8.00 GHz and with the ISPW mixture having a dielectric loss tangent of 0.48, the gain reduces to 3.20dBi (7.40 GHz). A slightly increased gain of 5.96 dBi is observed for the FR4 substrate (loss tangent of ~ 0.03) without the channels. While in the air filled case, because of the low loss tangent value, the substrate offers a higher gain of 6.21 dBi.

4.5 Discussion

Magnetically actuated microfluidic switches are employed for reconfiguration of the resonant frequency. The functional antenna offers alteration of frequency between two values by laterally shifting the dielectric liquids through a contactless actuator. The two distinct resonances also have significant gain and beam width comparable to that of a standard RMA. The approach demonstrates a simple and effective technique to convert an RMA into a frequency reconfigurable antenna without disturbing the profile of the radiating patch. In this design absence of biasing lines, required for electronic switches, has a positive effect on the antenna radiation pattern and makes them stable at both the frequencies resembling that of an RMA. The responses time of the switching is 358.19 milliseconds and within this time frame, the fluids interchange their positions. The design possess a significant advantage over most of the reported fluidic reconfiguration techniques [1, 7, 10, 11, 24-28] as it does not have any bulky mechanical pumping system. This will helps in reducing the overall form factor of the antenna.

References

[1] Bhattacharjee, T., Jiang, H., and Behdad, N. A Fluidically Tunable, Dual-Band Patch Antenna With Closely Spaced Bands of Operation. *IEEE Antennas and Wireless Propagation Letters,* 15:118-121, 2016. DOI:10.1109/LAWP.2015.2432575

[2] Murray, C., and Franklin, R.R. Independently Tunable Annular Slot Antenna Resonant Frequencies Using Fluids. *IEEE Antennas and Wireless Propagation Letters,* 13:1449-1452, 2014. DOI:10.1109/LAWP.2014.2341232

[3] Dey, A., and Mumcu, G. Microfluidically Controlled Frequency-Tunable Monopole Antenna for High-Power Applications. *IEEE Antennas and Wireless Propagation Letters,* 15:226-229, 2016. DOI:10.1109/LAWP.2015.2438863

[4] Huff, G.H., Rolando, D.L., Walters, P., and McDonald, J. A Frequency Reconfigurable Dielectric Resonator Antenna Using Colloidal Dispersions. *IEEE Antennas and Wireless Propagation Letters,* 9:288-290, 2010. DOI:10.1109/LAWP.2010.2046613

[5] Entesari, K., and Saghati, A.P. Fluidics in Microwave Components. *IEEE Microwave Magazine,* 17(6):50-75, 2016. DOI:10.1109/MMM.2016.2538513

[6] Khan, M.R., Hayes, G.J., So, J.-H., Lazzi, G., and Dickey, M.D. A frequency shifting liquid metal antenna with pressure responsiveness. *Applied Physics Letters,* 99(1):013501, 2011. DOI:10.1063/1.3603961

[7] Kim, D., Pierce, R.G., Henderson, R., Doo, S.J., Yoo, K., and Lee, J.-B. Liquid metal actuation-based reversible frequency tunable monopole antenna. *Applied Physics Letters,* 105(23):234104, 2014. DOI:10.1063/1.4903882

[8] King, A.J., Patrick, J.F., Sottos, N.R., White, S.R., Huff, G.H., and Bernhard, J.T. Microfluidically Switched Frequency-Reconfigurable Slot Antennas. *IEEE Antennas and Wireless Propagation Letters,* 12:828-831, 2013. DOI:10.1109/LAWP.2013.2270940

[9] Morales, D., Stoute, N.A., Yu, Z., Aspnes, D.E., and Dickey, M.D. Liquid gallium and the eutectic gallium indium (EGaIn) alloy: Dielectric functions from 1.24 to 3.1 eV by electrochemical reduction of surface oxides. *Applied Physics Letters,* 109(9):091905, 2016. DOI:10.1063/1.4961910

[10] Morishita, A.M., Kitamura, C.K.Y., Ohta, A.T., and Shiroma, W.A. A Liquid-Metal Monopole Array With Tunable Frequency, Gain, and Beam Steering. *IEEE Antennas and Wireless Propagation Letters,* 12:1388-1391, 2013. DOI:10.1109/LAWP.2013.2286544

[11] Rodrigo, D., Jofre, L., and Cetiner, B.A. Circular Beam-Steering Reconfigurable Antenna With Liquid Metal Parasitics. *IEEE Transactions on Antennas and Propagation,* 60(4):1796-1802, 2012. DOI:10.1109/TAP.2012.2186235

[12] Wang, M., Trlica, C., Khan, M.R., Dickey, M.D., and Adams, J.J. A reconfigurable liquid metal antenna driven by electrochemically controlled capillarity. *Journal of Applied Physics,* 117(19):194901, 2015. DOI:10.1063/1.4919605

[13] Christodoulou, C.G., Tawk, Y., Lane, S.A., and Erwin, S.R. Reconfigurable antennas for wireless and space applications. *Proceedings of the IEEE,* 100(7):2250-2261, 2012.

[14] Devi, M., and Mohanta, D. Rheological Properties of Iron Oxide Based Ferrofluids. *AIP Conference Proceedings,* 1147(1):495-501, 2009. DOI:10.1063/1.3183480

[15] Furumura, K., and Matsunaga, S., "Process for producing a ferrofluid, and a composition thereof," 1984.

[16] Jubb, A.M., and Allen, H.C. Vibrational spectroscopic characterization of hematite, maghemite, and magnetite thin films produced by vapor deposition. *ACS Applied Materials & Interfaces,* 2(10):2804-2812, 2010.

[17] Baker-Jarvis, J., D. Janezic, M., John H, J.G., and G. Geyer, R. *Transmission/Reflection and Short-circuit Line Methods for Measuring Permittivity and Permeability.* 1992.

[18] Baker-Jarvis, J., Vanzura, E.J., and Kissick, W.A. Improved technique for determining complex permittivity with the transmission/reflection method. *IEEE Transactions on Microwave Theory and Techniques,* 38(8):1096-1103, 1990. DOI:10.1109/22.57336

[19] Gogoi, P.G. *Design and development of compact flexible wearable antenna for c band communications*. PhD Thesis, Physics, Tezpur University, Tezpur, 2016.

[20] Chen, L.-F., Ong, C., Neo, C., Varadan, V., and Varadan, V.K. *Microwave electronics: measurement and materials characterization.* John Wiley & Sons. 2004.

[21] Nicolson, A.M., and Ross, G.F. Measurement of the Intrinsic Properties of Materials by Time-Domain Techniques. *IEEE Transactions on Instrumentation and Measurement,* 19(4):377-382, 1970. DOI:10.1109/TIM.1970.4313932

[22] Balanis, C.A. *ANTENNA THEORY: ANALYSIS AND DESIGN, 3RD ED (With CD).* Wiley India Pvt. Limited. 2009.

[23] Garg, R. *Microstrip Antenna Design Handbook.* Artech House. 2001.

[24] Bhattacharjee, T., Jiang, H., and Behdad, N. Fluidic beam steering in parasitically coupled patch antenna arrays. *Electronics Letters,* 51(16):1229-1231, 2015. DOI:10.1049/el.2015.1908

[25] Saghati, A.P., Batra, J., Kameoka, J., and Entesari, K. A microfluidically-tuned dual-band slot antenna. in *2014 IEEE Antennas and Propagation Society International Symposium (APSURSI)*, 1244-1245, 2014.

[26] Wang, C., Yeo, J.C., Chu, H., Lim, C.T., and Guo, Y. Design of a Reconfigurable Patch Antenna Using the Movement of Liquid Metal. *IEEE*

Antennas and Wireless Propagation Letters, 17(6):974-977, 2018. DOI:10.1109/LAWP.2018.2827404

[27] Konca, M., and Warr, P.A. A Frequency-Reconfigurable Antenna Architecture Using Dielectric Fluids. *IEEE Transactions on Antennas and Propagation,* 63(12):5280-5286, 2015. DOI:10.1109/TAP.2015.2490243

[28] Chen, Z., and Wong, H. Liquid Dielectric Resonator Antenna With Circular Polarization Reconfigurability. *IEEE Transactions on Antennas and Propagation,* 66(1):444-449, 2018. DOI:10.1109/TAP.2017.2762005